Impact localization in composite structures of arbitrary cross-section

F. Ciampa[1], M. Meo[1*] and E. Barbieri[2]

[1]Department of Mechanical Engineering, University of Bath, Bath BA2 7AY, UK

[2]Department of Engineering Science, University of Oxford, Oxford OX1 3PJ, UK

Abstract

This paper proposes an *in-situ* Structural Health Monitoring (SHM) method able to locate the impact source and to determine the flexural Lamb mode A_0 velocity in composite structures with unknown lay-up and cross-section. The algorithm is based on the differences of the stress waves measured by six surface attached acoustic emission piezoelectric (PZT) sensors and is branched off into two steps. In the first step, the magnitude of the Continuous Wavelet Transform (CWT) squared modulus, which guarantees high accuracy in the time-frequency analysis of the acoustic waves, was used to identify the arrival time (TOA) of the flexural Lamb wave. Then, the coordinates of the impact location and the group speed values are obtained by solving a set of non-linear equations through a combination of local Newton's iterative method associated to line search and polynomial backtracking techniques. The proposed method, in contrast to the current impact localization algorithms, does not require *a priori* knowledge of the anisotropy angular-group velocity pattern of the measured waveforms as well as the mechanical properties of the structure. To validate this method, experimental location testing were conducted on two different composite structures, a quasi-isotropic CFRP

* Corresponding author: m.meo@bath.ac.uk

laminate and a sandwich panel. The results showed that source location was achieved with satisfactory accuracy (maximum error in estimation of the impact location was approximately 3 mm for quasi-isotropic carbon fibre reinforced plastic (CFRP) panel and nearly 2 mm for sandwich plate), requiring little computational time (nearly 1 sec). In addition, the values of the fundamental flexural Lamb mode A_0 obtained from the optimization algorithm were compared with those determined by a numerical spectral finite element method.

Keywords: impact location identification, composite structures, Continuous Wavelet Transform, Lamb waves.

1 Introduction

Due to their desirable characteristics as high strength, stiffness and low weight, advanced composite structures have been widely used over recent years in aerospace and civil applications. However, the mechanical properties of such materials can be severely degraded after an external impact, which might occur during service or maintenance. Structural health monitoring (SHM) systems based on guided waves with integrated components (passive sensors and probes) are addressed to provide a real-time warning of the structural health status and to avoid the tested specimen to be disassembled during the inspections. In this manner, disruptions and a considerable increse in maintenance costs can be eluded. In isotropic or quasi-isotropic materials, the impact source location is conventionally performed through a time of arrival (TOA) triangulation technique (also known as Tobias algorithm) [1, 2, 3]. However, since the group velocity in isotropic media is assumed constant in all direction, these methods are

not suitable for anisotropic and inhomogeneous structures. In the last decade, a number of studies present in literature were focused to the detection and location of the acoustic emission (AE) source (impact event) in composite materials. White [4] was one of first to look into arrival time measurements in dispersive media, whilst Ziola et al. [5] employed wavelets to determine arrival times in dispersive media. Seydel and Chang [6] proposed a *model-based method* for the reconstruction of the force history and the identification of the impact location, based on the minimization of the difference between the actual and predicted response from PZT. Although this method was applied to any kind of anisotropic material, even with complex geometries, it required the knowledge of the mechanical properties of the medium and a theoretical model for the simulation of dynamic-acoustic behaviour of the structure. Meo et al. [7], Paget et al. [8] and Kurokawa et al. [9] developed an algorithm for the impact point identification assuming an elliptical angular-group velocity pattern. This method necessitated a priori knowledge of the group velocities at 0 and 90 degrees with respect to the planar reference frame *x-y*, and it was applied to only quasi-isotropic and unidirectional composite structures. Kundu et al [10] presented an alternative approach that consisted of minimizing an error function representing the differences of TOA of the recorded signals. Huang et al [11] used nonlinear least squares optimization methods to calculate laminated plate stiffnesses from measured group velocities.

This paper extends a previous work for isotropic materials [12], which demonstrated that with four sensors the impact location and the group velocity could be uniquely evaluated. It presents an in-situ SHM system able to pinpoint the impact source location and to determine the group speed of the flexural Lamb mode A_0 in composite plate-like structures. This research work is based on the differences of the wave packets measured

by six surface bonded AE piezoelectric (PZT) sensors, and it can be applied to composite laminates with any lay-up, thickness and anisotropic angular-group velocity pattern. In a first step, the time of arrivals were obtained through a suitable signal processing based on the magnitude of the Continuous Wavelet Transform (CWT) squared modulus. Then, the coordinates of the impact location and the group speed were determined by solving a set on nonlinear equations through a combination of local Newton's method associated to global unconstrained optimization (line search and polynomial backtracking techniques). Therefore, this algorithm overcomes the limitations of most impact detection systems, as it does not require *a-priori* knowledge of the anisotropic group velocity as well as the mechanical properties and the orientation of each ply in the laminate. Moreover, the CWT guarantees high accuracy in the time-frequency analysis of the acoustic waveform, since it is able to characterize near Lamb modes. In fact, the group speed is not constant but dependent of the excitation frequency and the heading angle in the *x-y* plane [$V_g = V_g(f, \theta)$]. To validate this method, a number of experiments on a quasi-isotropic CFRP laminate and a sandwich panel were carried out. Fig. 1 illustrates the architecture of the impact location algorithm.

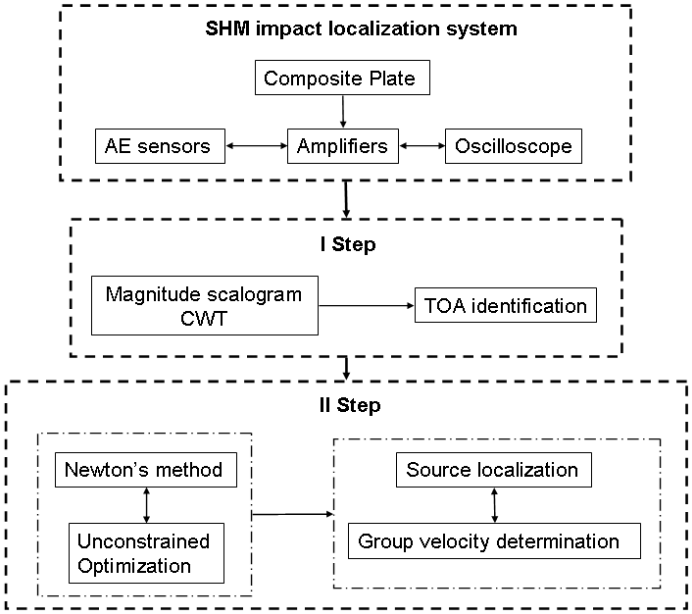

Figure 1 Architecture of the SHM impact localization system

The layout of the paper is as follow: in Section 2 the algorithm for the impact source localization and the fundamental flexural Lamb wave speed determination is presented. Section 3 describes the procedure for identifying the time of arrival using the Continuous Wavelet Transform. In Section 4, the optimization algorithm for obtaining the coordinates of the impact point is discussed. Section 5 reports the experimental set-up, whilst in Section 6 the impact source location results for both CFRP and sandwich composite plate are reported. Then, the conclusions of the method adopted are outlined.

2 Impact localization algorithm

Mathematically, locating an impact source is an inverse problem. Let us consider the impact source point *I* is at unknown coordinates (x_I, y_I) in the plane of the plate *x*-*y*. The transducers are located at distance l_i $(i = 1,\ldots,6)$ from the source, and d_{km} $(k = 1,3,5)$ $(m = 2,4,6)$ are the distances between each pair of transducers *k* and *m* (Fig. 2). Furthermore, the dimensions of the plate are *L,* length and *W*, width.

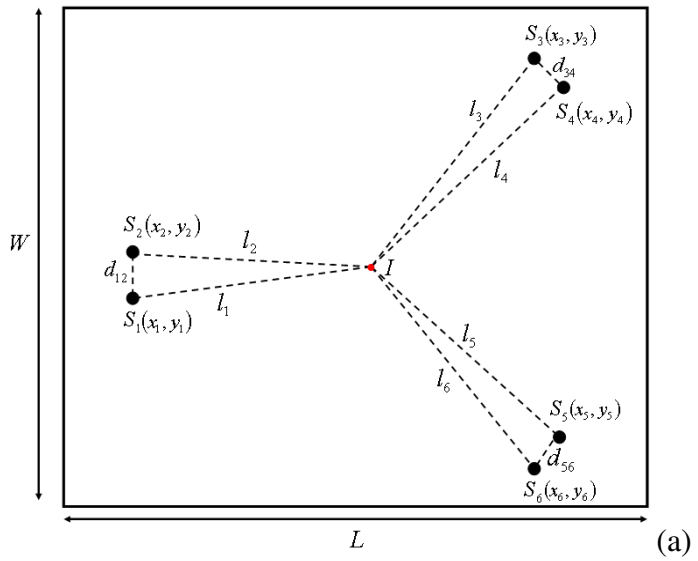

Figure 2 (a) (b) Sensors arrangement for the source location (a) and optimal disposition with short distance of each pair of transducers (b)

The coordinates of the acoustic emission source can be determined by solving the following equations:

$$\begin{cases} \|\mathbf{l}_i\|^2 = (x_i - x_I)^2 + (y_i - y_I)^2 \\ t_i = \dfrac{\|\mathbf{l}_i\|}{V_{g,i}} \end{cases} \tag{1}$$

where $V_{g,i}$ is the velocity of propagation of the stress wave reaching the *i-th* transducer, t_i is the time of detection of the AE signals and (x_i, y_i) are the coordinates of the *i-th* sensor. Combining both terms of equation (1), the following system of six equations for 14 unknowns (t_i, x_I, y_I and $V_{g,i}$) can be obtained:

$$(x_i - x_I)^2 + (y_i - y_I)^2 - (t_i V_{g,i})^2 = 0 \tag{2}$$

which represents the equation of circumferences with radius $r_i^2 = \left(t_i V_{g,i}\right)^2$. However, if t_1 is the travel time required to reach the sensor 1 (*master sensor*) and Δt_{1j} $\left(j = 2,\ldots,6\right)$ are the time difference between sensor *j* and the master one, we can write:

$$t_j = t_1 \pm \Delta t_{1j} \tag{3}$$

Substituting equation (3) into (2), it becomes:

$$\left(x_i - x_I\right)^2 + \left(y_i - y_I\right)^2 - \left[\left(t_1 \pm \Delta t_{1j}\right)V_{g,i}\right]^2 = 0 \tag{4}$$

The above set of nonlinear equations cannot be solved yet since the number of variables is still bigger than the number of equations. Thereby, in order to find a solution of system (4), additional information is needed, i.e. an optimal sensors configuration. In the current approach, the sensors were located so that each pair of transducers was relatively close together (see Fig. 2-a). In this manner, any pair will experience approximately the same group speed. Therefore, based on the sensors configuration as depicted in Fig. 2-b, if $l_1, l_2 >> d_{12}$, we have:

$$\frac{d_{12}}{l_1} \approx \sin\left(\underbrace{\theta_1 - \theta_2}_{\Delta\theta}\right) << 1 \tag{5}$$

where d_{12} is the distance between sensors 1-2, l_1 and l_2 are the distances from the impact source and θ_1 and θ_2 are the heading angles (propagation angles) of the AE in the reference frame. Hence, if $\Delta\theta = \theta_1 - \theta_2$ is sufficiently small (close transducers) such that $\theta_1 \approx \theta_2$, the following assumption becomes straightforward:

$$\begin{cases} V_{g,1}(\theta) \approx V_{g,2}(\theta) \\ V_{g,3}(\theta) \approx V_{g,4}(\theta) \\ V_{g,5}(\theta) \approx V_{g,6}(\theta) \end{cases} \tag{6}$$

Thereby, system (5) can now be rewritten as:

$$\left(x_i - x_I\right)^2 + \left(y_i - y_I\right)^2 - \left[\left(t_1 \pm \Delta t_{1j}\right)V_{g,k}\right]^2 = 0 \text{ with } k = 1,3,5 \qquad (7)$$

Source location and group velocity of the flexural Lamb mode can now be calculated by solving the above set of six nonlinear equations with the six unknowns $\mathbf{x} = \left\{x_I, y_I, t_1, V_{g,1}, V_{g,3}, V_{g,5}\right\}$. Therefore, since no mechanical properties and simple angular-group speed pattern are required, the proposed technique is able to obtain the source location in anisotropic structures for arbitrary lay-up or thickness of the plate. However, an appropriate time-frequency analysis for the determination of the time differences Δt_{1j} as well as a well-adapted localization algorithm needs to be chosen.

3 Time of arrival identification using the Continuous Wavelet Transform

The dispersive nature of the flexural Lamb mode and the uncertainty of the noise level can drastically decrease the performance of a source localization system. Hence, a good impact detection method necessitates of a suitable choice of the time–frequency analysis for the TOA. A wavelet transformation method was chosen as it provides a good compromise between time and frequency resolution, and it is able to analyze low and high frequencies at the same time, even respecting the *uncertainty principle* (also known as *Heisenberg inequality*) [13]. The Continuous Wavelet Transform (CWT) is a linear transform that correlates the harmonic waveform $u(x,t)$ with basis functions that are simply dilatations and translations of a mother wavelet $\psi(t)$, by the continuous convolution of the signal and the scaled or shifted wavelet [14]:

$$WT(x,a,b) = \frac{1}{\sqrt{a}}\int_{-\infty}^{+\infty} u(x,t)\psi^*\left(\frac{t-b}{a}\right)dt \qquad (8)$$

where $\psi^*(t)$ denotes the complex conjugate of the mother wavelet $\psi(t)$, a is the dilatation or scale parameter defining the support width of the wavelet and b the translation parameter localising the wavelet in the time domain.

A number of mother wavelets existing in literature have been widely used for the acoustic emission localization in isotropic and anisotropic structures [1,2 and 7]. In this study, the complex Morlet wavelet was employed as it is able to separate amplitude and phase, enabling the measurement of instantaneous frequencies and their temporal evolution. The complex Morlet wavelet is expressed by the following equation [13]:

$$\psi(t) = \frac{1}{\sqrt{\pi F_b}} e^{j\omega_c t} e^{-\frac{t^2}{F_b}} = \frac{1}{\sqrt{\pi F_b}} e^{-\frac{t^2}{F_b}} \left[\cos(\omega_c t) + j\sin(\omega_c t)\right] \qquad (9)$$

where $f_c = \omega_c / 2\pi$ is the *central frequency* and F_b the *shape control parameter* (wavelet bandwidth). For practical purposes, because of the fast decay of the Morlet wavelet's envelope towards zero, such function is considered admissible for ω_c=6. In addition, F_b was chosen equal to 0.1.

The waveforms recorded are analyzed in terms of group (energy) velocity–frequency relationship. The group velocity is defined as the velocity of a modulated wave that is constructed considering a time harmonic motion of two waves of unit amplitude with slightly different frequencies ω_1 and ω_2 propagating in the x-direction of a thin plate as follows [2, 15]:

$$u(x,t) = e^{-j(k_1 x - \omega_1 t)} + e^{-j(k_2 x - \omega_2 t)} \qquad (10)$$

where k_1 and k_2 are the wave numbers. Introducing $(k_1 + k_2)/2 = k_0$, $(k_1 - k_2)/2 = \Delta k$, $(\omega_1 + \omega_2)/2 = \omega_0$ and $(\omega_1 - \omega_2)/2 = \Delta\omega$, equation (10) becomes:

$$u(x,t) = 2\cos\left[\Delta k x - \Delta\omega t\right] e^{-j(k_0 x - \omega_0 t)} \qquad (11)$$

Equation (11) is a modulated wave formed by a carrier $e^{-j(k_0x-\omega_0t)}$ with frequency ω_0 and the modulation $\cos[\Delta kx-\Delta\omega t]$ with frequency $\Delta\omega$. The propagation velocity of the carrier is called phase velocity $V_{ph}=\omega_0/k_0$ and the propagation velocity of the envelope is called group velocity $V_g=d\omega/dk$ in the limit of $\Delta k\to 0$.

Substituting equation (10) in (8) using complex Morlet wavelet [eq. (8)], and assuming $\vartheta_1=\omega_1 b-k_1x$ and $\vartheta_2=\omega_2 b-k_2x$, we have:

$$WT(x,a,b)=\sqrt{a}\left[\hat{\psi}^*(a\omega_1)e^{j\vartheta_1}+\hat{\psi}^*(a\omega_2)e^{j\vartheta_2}\right] \tag{12}$$

The squared modulus of the CWT, also called a *scalogram*, indicates the energy density of the signal at each scale at any time [13, 16]. Hence, it is able to reveal the highest local energy content of the waveform $u(x,t)$ measured from each transducer. The squared modulus can be express as:

$$\left|WT(x,a,b)\right|^2=WT(x,a,b)\cdot WT^*(x,a,b) \tag{13}$$

Substituting equations (12) and its complex conjugate into (13), if $\Delta\omega$ is sufficiently small such that $\hat{\psi}(a\omega_1)\cong\hat{\psi}(a\omega_2)\cong\hat{\psi}(a\omega_0)$, we obtain:

$$\left|WT(x,a,b)\right|^2\approx 2a\left[\hat{\psi}(a\omega_0)\right]^2\left[1+\cos(\Delta\omega b-\Delta kx)\right] \tag{14}$$

Therefore, the above equation shows that the squared modulus of the CWT using complex Morlet wavelet reaches its peak value at $a=\dfrac{\omega_c}{\omega_0}$ and $b=\dfrac{\Delta k}{\Delta\omega}x=\dfrac{x}{V_g}$. Hence, it is demonstrated by equation (14) that the maximum value of the scalogram coefficients (ridges), obtained at the angular frequency of interest ω_0, allows identifying the time of arrival (b) of the group velocity V_g (Fig. 3).

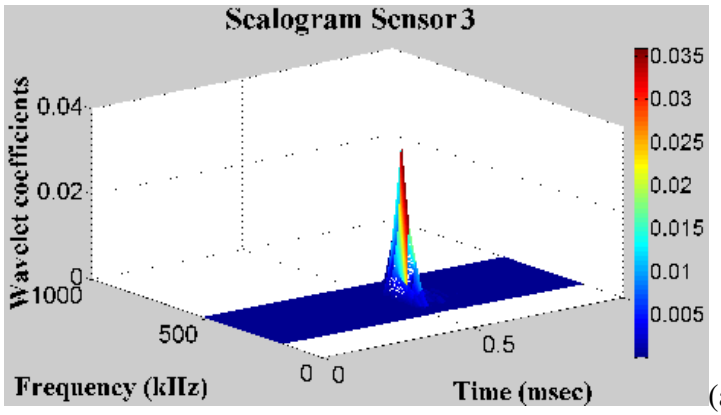

(a)

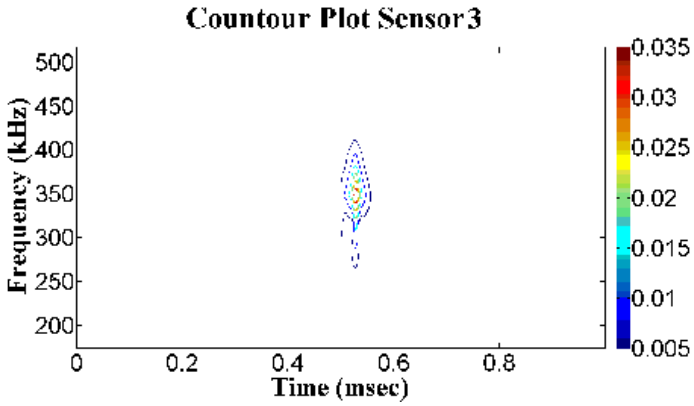

(b)

Figure 3 (a) (b) 3-D plot of the wavelet scalogram coefficients (a) and associated contour plot (b) of the recorded flexural wave

As depicted in Fig. 3-a, a red patch in the scalogram is representative of the ridge, i.e. the local energy content of the waveform recorded. Fig. 3-b shows that the red patch in the contour plot of the scalogram associated to the ridge is achieved at the instantaneous frequency $f_0 = 348.27$ kHz. The projection on the time domain of the ridge corresponds to the time of arrival (TOA) of the waves packets. Thus, the time differences Δt_{1j} with respect to the master sensor can be calculated and substituted in equation (7).

4 Newton's method and unconstrained optimization for solving systems on nonlinear equations

The method adopted for solving the set of equations (7) was to combine a Newton's method with an unconstrained optimization. Analogously to Ciampa and Meo [12], the set of nonlinear equations (7) can be expressed as:

$$\mathbf{F}(\mathbf{x}) = 0 \tag{15}$$

where $\mathbf{F}$ is the vector of the functions F_i ($i = 1,\ldots,6$) and $\mathbf{x}$ is the vector of unknowns x_j ($j = 1,\ldots,6$). Equation (15) has a zero at $\mathbf{x}^* \in \Re^n$ such that $\mathbf{F}(\mathbf{x}^*) = 0$. The iterate $\mathbf{x}^{n+1}$ from a current point $\mathbf{x}^n$ is given by [17]:

$$\mathbf{x}^{n+1} = \mathbf{x}^n + \delta\mathbf{x}^n = \mathbf{x}^n - \mathbf{J}(\mathbf{x}^n)^{-1} \cdot \mathbf{F}(\mathbf{x}^n) \tag{16}$$

where $\delta\mathbf{x} = \left[-\mathbf{J}(\mathbf{x})^{-1} \cdot \mathbf{F}(\mathbf{x})\right]$ is the Newton step and $\mathbf{J}(\mathbf{x})$ is the Jacobian matrix, which contains first derivatives of the objective function $\mathbf{F}(\mathbf{x})$ with respect to the six unknowns of the problem. However, in particular conditions, when the starting point $\mathbf{x}_0$ is not near the root, Newton's method may not converge [18]. The reasons for this failure are that the direction of the current iterate $\mathbf{x}^n$ might not be a direction of descent for $\mathbf{F}$, and, even if a search direction is a direction of decrease of $\mathbf{F}$, the length of the Newton step $\delta\mathbf{x}$ may be too long. Hence, the approach adopted in this paper was to combine the local Newton's method applied to the system (7) with the global unconstrained problem of minimizing the *objective function* $\mathbf{F}$:

$$\min_{x \in \Re^n} \mathbf{F} : \Re^n \to \Re \tag{17}$$

Among the class of powerful algorithms for unconstrained optimization, we focused on the Line-Search method and the polynomial backtracking technique [12] because of its simplicity, and because they do not depend on how the Jacobian is obtained. In

particular, the function to be minimized (also known as *merit function*) was the scalar-valued function of $\mathbf{F}$, i.e. the squared norm of $\mathbf{F}$:

$$\min_{x\in\Re^n} h(\mathbf{x}) = \min_{x\in\Re^n} \frac{1}{2}\|\mathbf{F}(\mathbf{x})\|^2 \tag{18}$$

where the factor $\frac{1}{2}$ is introduced for convenience. Obviously, any root of *h* fulfils the identity $h(\mathbf{x}^*)=0$. With this procedure, the computational time for each source location was about 1 sec (using a code written in Matlab on a standard PC), which means that the results can be obtained in quasi real-time using a compiled code.

5 Experimental set-up

To validate this algorithm, experimental location tests were conducted on two different composite structures simply supported at the edges:

- T300/914 carbon fibre reinforced plastic (CFRP) composite laminate with dimensions 502 mm x 437 mm x 6.94 mm and lay-up sequence of $[0/15/30/45/60/75/90]_{3s}$ (Fig. 4a). The ply properties are reported in Table 1.
- sandwich composite plate with dimensions of 380 mm long, 254 mm wide (Fig. 4-b). The core used in the sandwich was a 6.35 mm thick HRH-10-1/8-4.0 Aramid fibre/phenolic resin nomex. Facing skins (2mm thick) were made of four plies of AS4/8552 unidirectional carbon/epoxy prepreg composite on both sides of the core with lay-up sequence of [90/45/45/90]. The ply and sandwich properties are reported in Tables 2 and 3.

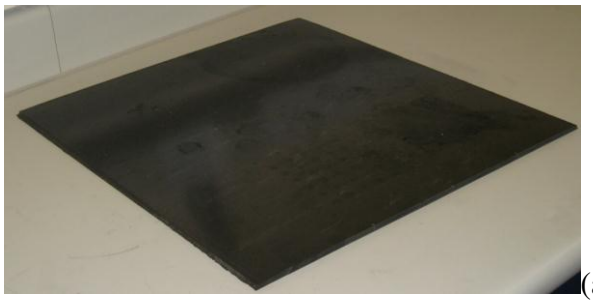
(a)

(b)

Figure 4 (a) (b) CFRP composite laminate (a) and sandwich plate (b).

Table 1 T300/914 mechanical properties

Young modulus E_{11} (GPa)	***Young modulus E_{22} (GPa)***	***Young modulus E_{33} (GPa)***	***Shear modulus G_{12} (GPa)***	***Shear modulus G_{23} (GPa)***	***Shear modulus G_{31} (GPa)$_z$***	***Poisson's ratio ν_{12}***	***Poisson's ratio ν_{13}***	***Poisson's ratio ν_{23}***
130	9.5	9.8	4.7	3.2	4.7	0.34	0.66	0.52

Table 2 AS4/8552 mechanical properties

Young modulus E_{11} (GPa)	***Young modulus E_{22} (GPa)***	***Young modulus E_{33} (GPa)***	***Shear modulus G_{12} (GPa)***	***Shear modulus G_{23} (GPa)***	***Shear modulus G_{31} (GPa)$_z$***	***Poisson's ratio ν_{12}***	***Poisson's ratio ν_{13}***	***Poisson's ratio ν_{23}***
122	9.8	9.8	5.12	5.12	3.35	0.26	0.26	0.47

Table 3 Sandwich core mechanical properties

Young modulus, compacted material (GPa)	***Transverse modulus (GPa)***	***Shear modulus, expansion (MPa)***	***Shear modulus, ribbon (MPa)***	***Poisson's ratio, compacted material***	***Densification strain***
1	0.41	89	44	0.25	0.8

The A_0 Lamb waves were generated using a hand–held modal hammer manufactured by Meggit-Endevco and were measured employing six acoustic emission sensors surface bonded with a central frequency of 300 kHz, provided by the courtesy of Airbus UK. Each sensing unit is aimed to provide high SNR ranging between 20 (please see Ch. 6 in Fig. 7) and 40 dB, and it is composed by acoustic emission sensors, preamplifiers used to convert high impedance AE-sensor signals into low impedance signals (50 Ohm), power supplies and pass-band filters, connected by low-noise cables (15 cm length).

The gain of the preamplifiers is 40 dB and their input impedance is 50 MOhm. Outputs of the transducers were connected to pass-band filters with a frequency range between 200 and 400 kHz and then linked to preamplifiers. According to the g_{31}/g_{32} electromechanical coupling mechanism of the acoustic emission sensors, at the mentioned finite bandwidth, only the fundamental antisymmetric Lamb wave A_0 was measured [19]. The signals were acquired using two four channels oscilloscopes with 16 bits of resolution and a sampling rate of 25 MHz. Both systems were synchronized in way that all the transducers were triggered by one of the sensors (master sensor). A Matlab software code implemented by the authors was written to analyze the waveforms with the wavelet transform and to find the impact location. Sensors location and impact source coordinates are reported in Table 4 for test 1 with CFRP (referred as impacts C1 C2 and C3 in the article) and Tables 5 and 6 for test 2 with sandwich plate (referred as impacts S1 S2 and S3 in the article).

Table 4 Sensors and impact coordinates in test 1, impacts C1 ,C2 and C3

	Sensor 1	***Sensor 2***	***Sensor 3***	***Sensor 4***	***Sensor 5***	***Sensor 6***	***Impact C1***	***Impact C2***	***Impact C3***
x-coordinate (mm)	120	110	250	280	430	420	280	270	420
y-coordinate (mm)	100	120	390	390	250	230	170	240	70
d_{km} (mm)	22.3		30		22.3				

Table 5 Sensors and impact coordinates in test 2, impact S1

	Sensor 1	***Sensor 2***	***Sensor 3***	***Sensor 4***	***Sensor 5***	***Sensor 6***	***Impact S1***
x-coordinate (mm)	120	110	190	210	320	330	210
y-coordinate (mm)	50	70	210	190	140	120	90
d_{km} (mm)	**22.3**		28.3		22.3		

Table 6 Sensors and impact coordinates in test 2, impact S2 and S3

	Sensor 1	***Sensor 2***	***Sensor 3***	***Sensor 4***	***Sensor 5***	***Sensor 6***	***Impact S2***	***Impact S3***
x-coordinate (mm)	100	90	170	190	310	290	190	50

y-coordinate (mm)	50	70	220	210	140	120	140	225
d_{km} (mm)	22.3		22.3		28.3			

6 Impact localization results

6.1 Source location results on CFRP laminate

As shown in Section 3, the signals were analyzed in terms of group velocity–frequency relationship and the peak of the scalogram was used to indicate the arrival time of the A_0 Lamb mode. The maxima coefficients in the experiments with a quasi-isotropic CFRP plate were found at the instantaneous frequency of 258.77 kHz. Fig. 5 illustrates the procedure for extracting the TOA at the above frequency of interest, for the configuration reported in test 1, impact C1. Fig. 6 shows the results of the source location for the impacts in test 1.

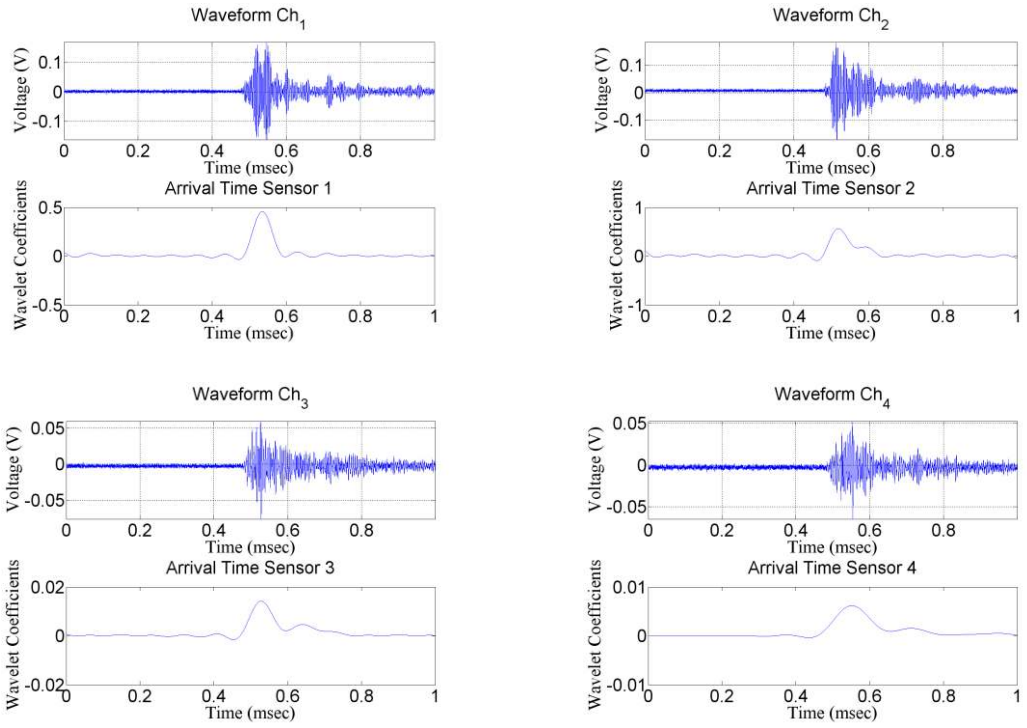

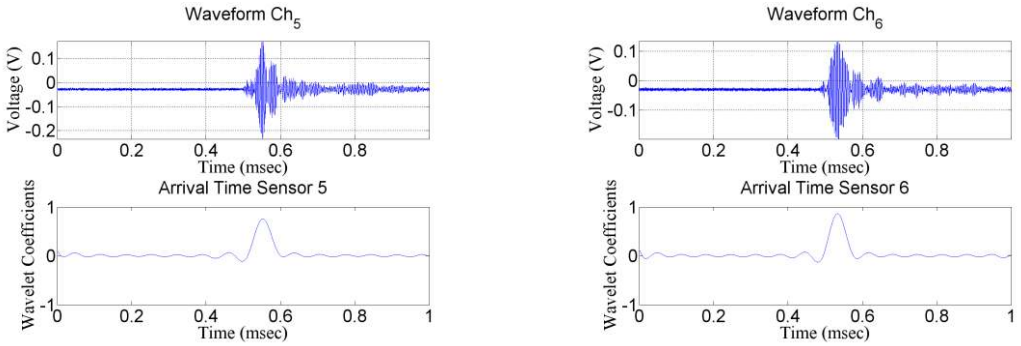

Figure 5 Time histories of the six recorded waveform (upper side) and the line profile of the scalogram (lower side) at the frequency $f_0 = 258.77$ kHz for the time of arrival identification in impact C1.

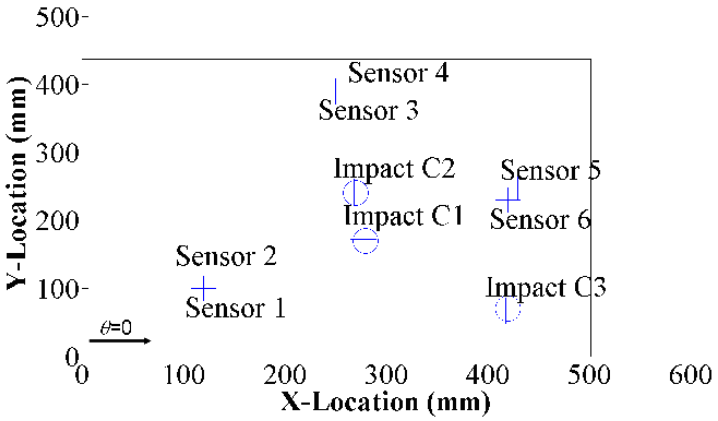

Figure 6 Source location results for impact C1, C2 and C3. The real (o) and calculated (*).

Table 7 depicts the evaluated impact positions and the error as expressed by the following formula:

$$\psi = \sqrt{\left(x_{real} - x_{calculated}\right)^2 + \left(y_{real} - y_{calculated}\right)^2} \qquad (18)$$

where $\left(x_{real}, y_{real}\right)$ are the coordinates of the real impact position and $\left(x_{calculated}, y_{calculated}\right)$ the coordinates of the impact location using the algorithm reported in Sections (1-4).

Table 7 Impact positions and errors for test 1

	Impact C1	**Impact C2**	**Impact C3**
x-coordinate source location (from algorithm) [mm]	277.56	268.32	417.89
x-coordinate source location (real value) [mm]	280	270	420
y-coordinate source location (from algorithm) [mm]	172.43	242.12	67.35
y-coordinate source location (real value) [mm]	170 m	240	70
Location error ψ [mm]	3.44	2.7	3.38

As it can be seen from Table 7, this algorithm provides results with satisfactory accuracy (maximum error in estimation of the coordinates of the impact location was

approximately 3 mm) for all the impacts considered, even outside the area defined by the sensors.

6.2 Source location results on sandwich panel

The scalogram maxima coefficients in both experiments with the sandwich plate were found at the instantaneous frequency of 348.27 kHz. Fig. 7 illustrates the procedure for extracting the TOA at the above frequency of interest, for the configuration reported in test 2, impact S1.

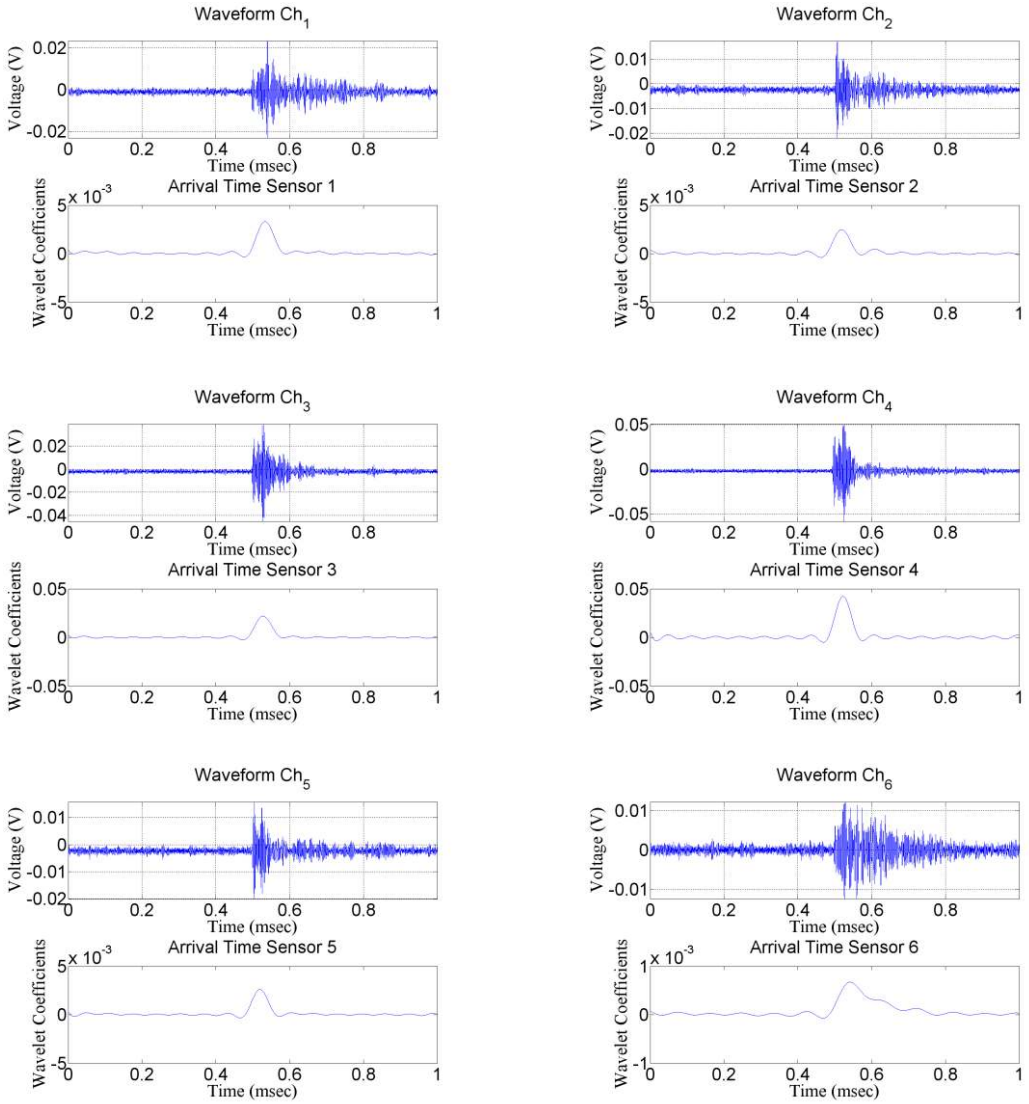

Figure 7 Time histories of the six recorded waveform (upper side) and the line profile of the scalogram (lower side) at the frequency $f_0 = 348.27$ kHz for the time of arrival identification in impact S1.

Fig. 8 shows the results of the source location for both impacts in test 2. As in Fig. 6, the real source location is represented by an open circle (o), whilst the calculated source impact position is illustrated by a star symbol (*). Table 8 depicts the evaluated impact positions and the errors.

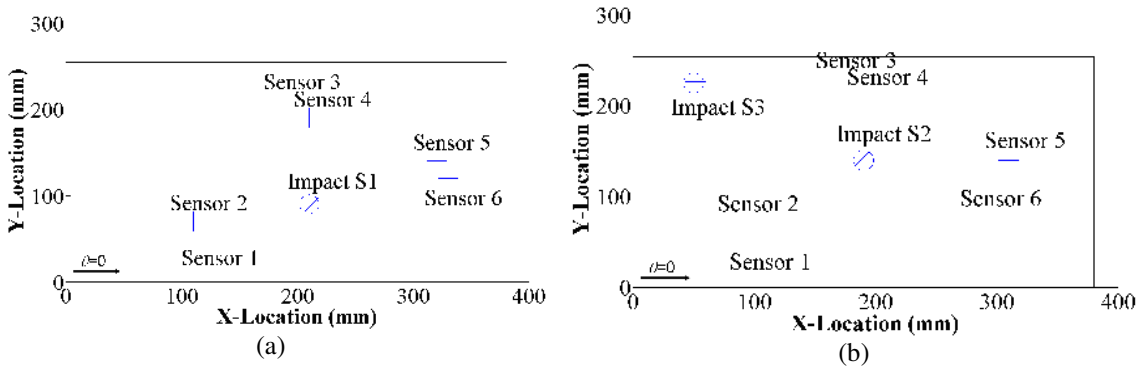

Figure 8 (a) (b) Source location results for impact S1 (a) and S2, S3 (b). The real (o) and calculated (*).

Table 8 Impact positions and errors for test 2

	Impact S1	**Impact S2**	**Impact S3**
x-coordinate source location (from algorithm) [mm]	211.71	188.23	51.67
x-coordinate source location (real value) [mm]	210	190	50
y-coordinate source location (from algorithm) [mm]	89.18	141.07	226.45
y-coordinate source location (real value) [mm]	90	140	225
Location error ψ [mm]	1.89	2.07	2.21

As it can be seen from the above table, this algorithm generates results with reasonable accuracy (maximum error in estimation of the coordinates of the impact location was approximately 2 mm) even in complex structures as sandwich panels. In the experiments on both CFRP and sandwich plate, according to eq. (5), the maximum distance between any pair of sensors was assumed equal to approximately one third of the distance of the closest transducer from the impact location (e.g. see d_{34} in Tab. 6 and l_4 in Tab. 11 for impact S2). The dimensions of the AE sensors (2 cm diameter) and the composite plate employed were such that the $\Delta\theta$ was sufficiently small to guarantee the same group speeds for each pair of transducers.. In addition, it was observed during

the test on the sandwich plate that due to the severe attenuation in the resin core, the peak magnitude of the scalogram for each pair of transducers occurred at slightly different frequencies (within a band Δf_0 of 10 Hz) with respect to the nominal value of 348.27 kHz. This means that the TOA evaluation error due to this frequency shift was negligible.

6.3 Group velocity results on CFRP laminate

The values of the fundamental flexural Lamb mode A_0 obtained from the optimization algorithm were compared with those determined by a semi-analytical finite element (SAFE) approach also known as spectral finite element (SFEM) method. The SFEM algorithm for undamped media presented by Barbieri et al. [20] was extended to obtain the dispersion relations of group velocity for the most common composite structures of arbitrary thickness. This technique provides a description of the cross-sectional deformation of a laminate using a finite element discretization of the cross-sectional displacement field. The displacements were approximated as harmonic exponential functions with the shape independent of frequency and a one-dimensional FE mesh along the thickness was assumed. The characteristic equation (SFEM solution) for free wave propagation was obtained in stable manner from a linear eigenvalue problem in wavenumber *k*. With this method, the propagating wave field can be predicted for any kind of composite laminate. The approach proposed by Finnveden [21] was used as it allowed obtaining the group velocity at each frequency and wavenumber solution, without the need to calculate the differentiations of two close frequencies and two adjacent wave numbers [see eq. (11)]. Table 9 provides the values of the group velocities calculated from the algorithm in the CFRP laminate, whilst Fig. 9 illustrates

the dispersion curves for the Lamb wave A_0 and the angular-dispersion pattern at the instantaneous frequency of 258.77 kHz.

Table 9 Flexural Lamb mode group velocity results for test 1

		Impact C1	Impact C2	Impact C3
Group velocity (from algorithm)	Sensors 1-2 (m/s)	1618.32	1617.22	1621.46
	Sensors 3-4 (m/s)	1624.56	1622.12	1617.87
	Sensors 5-6 (m/s)	1616.44	1619.78	1619.07

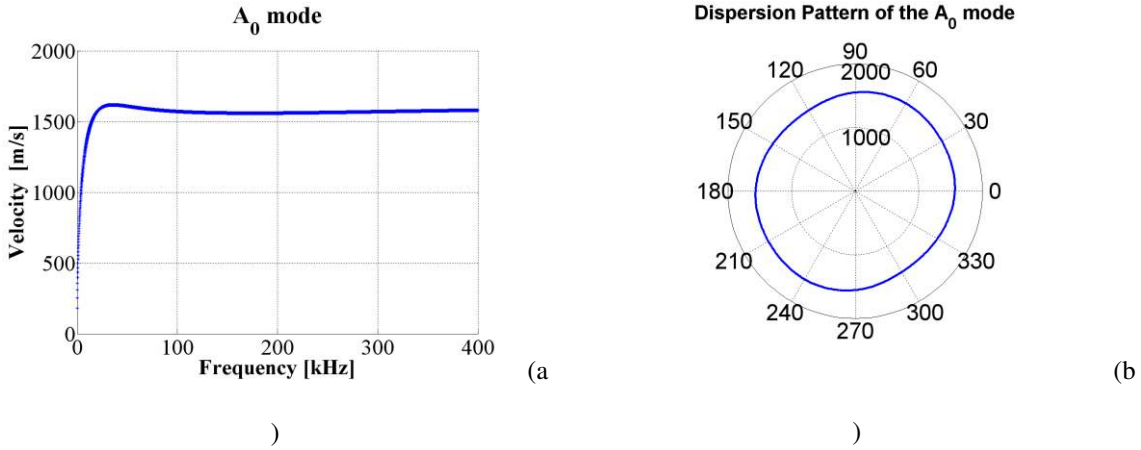

(a) (b)

Figure 9 (a) (b) Dispersion curves for the A_0 flexural Lamb mode at $\theta = 0$ (a) and angular-group velocity pattern at 258.77 kHz (b)

According to the quasi-isotropic nature of the CFRP composite plate, the angular-group velocity pattern was nearly circular (Fig. 9-b) and the A_0 Lamb mode calculated by the algorithm for any pair of transducers was approximately the same (close to the value of 1620 m/s, i.e. the maximum value for A_0 reported in Fig. 9-a).

6.4 Group velocity results on sandwich plate

In relation to the previous section, the group speeds values obtained from the optimization algorithm were compared with those determined by the SFEM method for the sandwich plate. Table 10 reports the group velocities calculated from the algorithm, whilst in Fig. 10 the dispersion curves for the Lamb wave A_0 and the angular-dispersion pattern at the instantaneous frequency of 348.27 kHz are displayed.

Table 10 Flexural Lamb mode group velocity results for test 2

		Impact S1	Impact S2	Impact S3
Group velocity (from algorithm)	Sensors 1-2 (m/s)	2810.08	2768.15	3117.45
	Sensors 3-4 (m/s)	3200.23	3078.86	2987.23
	Sensors 5-6 (m/s)	2840.74	2924.43	3002.29

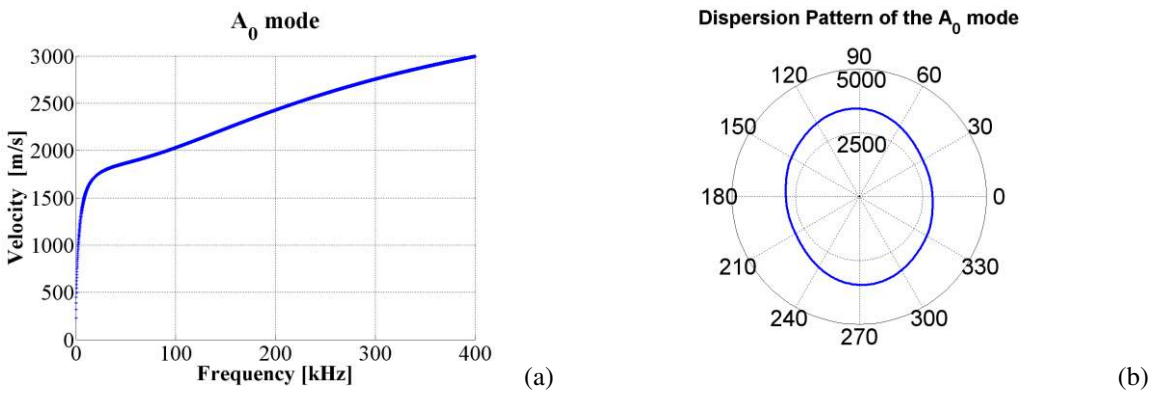

(a) (b)

Figure 10 (a) (b) Dispersion curves for the A_0 flexural Lamb mode at $\theta = 0$ (a) and angular-group velocity pattern at 348.27 kHz (b)

Although the calculated group velocity matched very well with those obtained from the dispersion curves in the CFRP case (Table 9 and Fig. 9), for the sandwich plate the predicted values from the algorithm were slightly different from the reconstructed response provided by the SFEM model (Table 10 and Fig. 10). Indeed, as it can be seen from Fig. 10-a, the value of the flexural group velocity at 348.27 kHz is approximately 2800 m/s. This is mainly due to the high attenuations in the sandwich core that are not included in the SFEM model.

However, this qualitative comparison of the fundamental flexural velocity was useful to highlight the drawbacks related to the A_0 Lamb wave speed evaluation through numerical methods, especially in complex structures (sandwich panel). Therefore, this algorithm proved to be an efficient way to overcome the drawbacks related to the uncertainty of the group estimation provided by the dispersion curves, and the limits of

a-priori prediction with an accurate model of the structural response of complex structures.

Conclusions

This research work shows an *in-situ* Structural Health Monitoring (SHM) method for locating the acoustic emission source (impact event) and for determining the velocity of elastic waves in plate-like composite structures. The proposed method is based on the differences of the stress waves measured with high SNR by six surface attached acoustic emission PZT sensors. The peak magnitude of the scalogram was employed to identify the arrival time (TOA) of the flexural A_0 Lamb mode. The coordinates of the impact location and the group speed were obtained by solving a set of non-linear equations through a combination of local Newton's iterative method associated to a global unconstrained optimization (line search and polynomial backtracking technique). This algorithm does not require *a priori* knowledge of the anisotropy angular-group velocity pattern of the AE waveforms as well as the mechanical properties, lay-up and thickness of the structure. The experimental results conducted on a quasi-isotropic CFRP laminate and a sandwich panel showed that the identification of the source location was achieved with satisfactory accuracy (maximum error in estimation of the impact location was approximately 3 mm for quasi-isotropic CFRP panel and nearly 2 mm for sandwich plate). Moreover, a comparison between the group velocities calculated by the algorithm and the values obtained from the dispersion curves through a SFEM method was accomplished.

Acknowledgements

Funding for this research work was provided by Airbus UK and Great Western Research.

Appendix 1

Table 11 reports the distances between the sensors and the impact location for all the experiments carried out (test 1 and 2).

Table 11 Sensors and impact distances for test 1 and 2

	l_1 (mm)	l_2 (mm)	l_3 (mm)	l_4 (mm)	l_5 (mm)	l_6 (mm)
Impact C1	174.6	177.2	222	220	170	152.3
Impact C2	205.2	200	151.3	150.3	160.3	150.3
Impact C3	301.5	314	362.3	349.3	180.3	160
Impact S1	98.5	102	121.6	100	120.8	123.7
Impact S2	127.3	122.1	82.5	70	120	102
Impact S3	182	160	120.1	140.8	273.5	262

Table 12 illustrates the time of arrivals of the waveforms reaching the *i-th* sensor calculated by the algorithm for test 1 and 2.

Table 12 Time of arrivals calculated from the algorithm for test 1 and 2

	t_1 (msec)	t_2 (msec)	t_3 (msec)	t_4 (msec)	t_5 (msec)	t_6 (msec)
Impact C1	0.107	0.108	0.134	0.133	0.105	0.095
Impact C2	0.127	0.123	0.0919	0.0914	0.099	0.093
Impact C3	0.184	0.192	0.224	0.217	0.113	0.1
Impact S1	0.035	0.036	0.038	0.031	0.042	0.043
Impact S2	0.045	0.043	0.026	0.022	0.041	0.035
Impact S3	0.058	0.051	0.04	0.046	0.09	0.086

References

[1] Gaul L, Hurlebaus S, Jacobs L J. (2001). "Localization of a "synthetic" acoustic emission source on the surface of a fatigue specimen". *Research in Nondestructive Evaluation*, pp. 105-117.

[2] Jeong H, Jang Y-S. (2000). "Fracture source location in thin plates using the wavelet transform of dispersive waves". *IEEE Transaction on Ultrasonics, Ferroelectrics, and Frequency Control*, **47**, pp.612-619.

[3] Tobias A. (1976). "Acoustic emission source location in two dimensions by an array of three sensors", *Non-Destructive Testing*, **9**, pp. 9-12.

[4] White P.H (1969). "Cross Correlation in Structural Systems: Dispersion and Nondispersion Waves", *Journal of the Acoustical Society of America, **45*** (*5*)*, pp.* 1118-1128.

[5] Ziola S M, Gorman M R. (1991). "Source location in thin plates using cross-correlation". *The Journal of the Acoustic Society of America **90*** (5), pp. 2551-2556

[6] Seydel R, Chang F K. (2001). "Impact identification on stiffened composite panels: system development". *Smart Materials and Structures **10***, pp. 354-369.

[7] Meo M, Zumpano G, Pigott M, Marengo G. (2005). "Impact identification on a sandwich plate from wave propagation responses". *Composite Structures **71***, pp. 302-306

[8] Paget C A, Atherton K, O'Brien E. (2003). "Triangulation algorithm for damage location in aeronautical composite structures". *Proceeding of the 4th International Workshop on Structural Health Monitoring, Stanford, CA*, pp. 363-370.

[9] Kurokawa Y, Mizutani Y, Mayozumi M. (2005). "Real-Time Executing source location system applicable to anisotropic thin structures". *Journal of Acoustic Emission* ***23***, pp. 224-232.

[10] Kundu T, Das S, J K V. (2009). "Detection of the point of impact on a stiffened plate by the acoustic emission technique". *Smart Materials and Structures* ***18***, pp. 1-9.

[11] Huang. W. (1998). "Stiffness Measurement and Defect Detection in Laminated Composites by Dry- Coupled Plate Waves", SPIE Symposium on Nondestructive Evaluation Techniques for Aging Infrastructure for Manufacturing, 31 March – 2 April, 1998, San Antonio, Texas.

[12] Ciampa F, Meo M. (2010). "Acoustic emission source localization and velocity determination of the fundamental mode A_0 using wavelet analysis and Newton-based optimization technique". *Smart Mater. Struct.* ***19***, 1-14.

[13] Teolis A. (1998). "Computational Signal Processing with Wavelets". Birkhauser, Boston, MA, USA.

[14] Mallat S. (1998). "A wavelet tour of signal processing". London: Academic Press.

[15] Bernard A, Lowe MJS, Deschamps M. (2000). "Guided waves energy velocity in absorbing and non-absorbing plates," *J. Acoust. Soc. Am.,* ***110***, 186–196.

[16] Haase M, Widjajakusuma J. (2003). "Damage identification based on ridges and maxima lines of the wavelet transform". *International Journal of Engineering Science* ***41***, pp. 1423-144.

[17] Dennis J E, Schnabel R B. (1983). "Numerical methods for unconstrained optimization and non linear equations". Englewood Cliffs, NJ: Prentice Hall.

[18] Nocedal J, Wright S J. (1999). “Numerical Optimization”. Springer Series in Operations Research.

[19] Tzou, H.-S. (2003).Piezoelectric Shells: Distributed Sensing and Control of Continua. Kluwer Academic Publishers, Boston/Dordrecht.

[20] Barbieri E, Cammarano A, De Rosa S, Franco F. (2009). “Waveguides of a Composite Plate by using the Spectral Finite Element Approach”. *J. Vibr. Contr., **15(3)**, pp.* 347–367.

[21] Finnveden, S. (2004). “Evaluation of modal density and group velocity by a finite element method” *J. Sound Vib. 273(**1**)*, pp. 51–75.